IEEE Access
Multidisciplinary | Rapid Review | Open Access Journal

Received 5 January 2024, accepted 12 January 2024, date of publication 16 January 2024, date of current version 1 February 2024.

Digital Object Identifier 10.1109/ACCESS.2024.3354842

RESEARCH ARTICLE

Behavioral Modeling of Direct-Conversion Receivers for Nonlinear Distortion Mitigation

CHONGCHONG CHEN[1], HONGMIN LU[1], (Member, IEEE), FULIN WU[1], XUAN LIU[1,2], AND YANGZHEN QIN[1]

[1]School of Electronic Engineering, Xidian University, Xi'an 710071, China
[2]China Academy of Space Technology, Xi'an 710100, China

Corresponding authors: Hongmin Lu (hmlu@mail.xidian.edu.cn) and Chongchong Chen (ccchen@stu.xidian.edu.cn)

ABSTRACT With the growing use of multicarrier technology in wireless communication, wideband receivers are facing increasingly severe nonlinear distortion issues. This paper focuses on the behavioral modeling of direct-conversion receivers (DCRs) for nonlinear distortion mitigation. This model accounts for arbitrary-order RF and baseband nonlinearities as well as the I/Q imbalance and can reproduce nonlinear distortion of the wideband DCR with multiple simultaneous input signals. Meanwhile, a method of model parameters estimation is put forward, which involves the inverse function method, singular value decomposition approach, and least square estimation. The experiment is performed by using a real RX chain and different types of input signals to evaluate the proposed model's accuracy in reproducing nonlinear distortions. The experimental and simulated results suggest that the proposed model can accurately reproduce signal distortions and intermodulation products (IMDs) of DCRs with several input signals of different modulations and power levels.

INDEX TERMS Nonlinear distortion, behavioral modeling, direct-conversion receiver (DCR), in-phase/quadrature (I/Q) imbalance, intermodulation distortion (IMD).

I. INTRODUCTION

With the advance of modern wireless communication systems, multi-technology scenarios, including multicarrier, multimode and multistandard technologies, are more and more popular, which drives the development towards multicarrier/multi-radio receivers where several carriers are received simultaneously through a single receiver [1], [2]. However, due to the non-ideality of analog components and the limitation of the receiver's dynamic range, the simultaneously received signals with various power levels may give rise to nonlinear distortion, which is likely to deteriorate the signal quality. Especially when the received signals contain strong signals/interferers and the weak desired signal, intermodulation products of strong signals/interferers can easily mask the weak desired signal. In addition, some intermodulation products may fall into free frequency bands and cause spurious responses and false alarms [3], [4].

In order to mitigate the nonlinear distortion in a receiver, much research has been undertaken for decades. References [5], [6], and [7] are dedicated to making some modifications to the receiver analog front-end to alleviate RF imperfections. These approaches have a remarkable effect on the mitigation of nonlinear distortion but need some specifications of front-end components and additional analog components, which in turn increases the cost, size, and power consumption of a receiver. Furthermore, the approaches in [8], [9], [10], and [11] adopt digital post-processing techniques to mitigate the nonlinear distortions, which exploit reference models to reproduce the nonlinear distortion products and then subtract them from the received signal. The key points to these approaches are a reference behavioral model to predict the receiver nonlinear distortion and the way to obtain its reference input. References [9] and [10] employ

The associate editor coordinating the review of this manuscript and approving it for publication was Mauro Fadda.

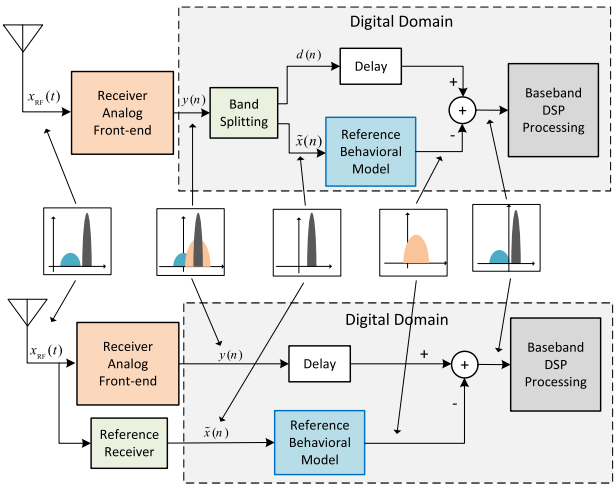

FIGURE 1. Block scheme for nonlinear distortion mitigation by using the band-splitting filter [10] and reference receiver [9].

a reference receiver and band-splitting filter respectively, to obtain the reference input for the behavioral model, both of which have a positive effect, as shown in Fig.1.

Therefore, a behavioral model that can accurately reproduce the nonlinear distortion of receivers is crucial, as it determines the effectiveness of these mitigation approaches. This paper focuses on behavioral modeling of nonlinear distortion of DCRs, which have been widely used in multistandard wireless communication systems due to their low power consumption and small size [2].

In the existing works of literature, there are many studies on nonlinear behavior modeling. Some studies focused on the nonlinear analysis and behavioral modeling of specific receiver components, such as amplifiers [12], [13], [14], [15], mixers [16], and ADCs [17]. Some studies focused on behavioral modeling of specific-order and partial nonlinearities of receivers and other nonlinear systems [6], [18], [19], [20], [21], [22]. References [9] and [10] adopted an adaptive filters-based model covering the RF and BB nonlinearities and I/Q imbalance of DCRs, but it requires the parameter estimation for each nonlinear distortion cancellation process, which results in a large computation amount, especially for higher-order nonlinearities. As a result, this model may not be suitable for higher-order nonlinearities and may not be efficient when used for distortion mitigation techniques. For optimal mitigation of receiver nonlinear distortion, a behavioral model is necessary to account for as much nonlinearity as possible.

This paper proposes a behavioral model of DCRs that can accurately reproduce nonlinear distortions. The model considers arbitrary-order RF and BB nonlinearities with memory effects, as well as I/Q imbalance. This model is more like an offline stable model where the model parameters are estimated only once before being applied for the nonlinear distortion mitigation process, which greatly reduces computation and improves efficiency. The outline of this paper is as follows. The nonlinearities of the DCR

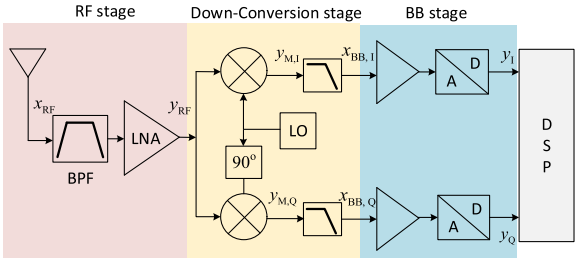

FIGURE 2. Conceptual DCR block diagram.

structure are analyzed and a behavioral model is proposed in Section II. In Section III, the process of estimating the model parameters is discussed. Section IV demonstrates the proposed model's validation by using a real RX chain in an experiment. The main conclusion of this paper is presented in Section V.

II. NONLINEARITIES MODELING

The block diagram in Fig.1 illustrates the conceptual DCR, which is divided into four main stages: the RF stage, the down-conversion stage, the BB stage, and the digital post-processing (DSP). The nonlinearity of DCRs mainly stems from non-ideal analog components in the receiver front end, including amplifiers, mixers, and ADCs. The RF stage filters incoming RF signals to remove out-of-band signals and amplify them through an LNA. In the down-conversion stage, RF signals are converted to BB signals via the I/Q mixer and then filtered by lowpass filters. In the BB stage, the BB signals are amplified to an appropriate voltage level and then digitalized through ADCs for further DSP processing.

For the input signal of DCRs, it can be presented as a bandpass signal

$$x_{\mathrm{RF}}(n) = \mathrm{Re}\left[x(n)\mathrm{e}^{j\omega_{\mathrm{c}}n}\right] = \frac{1}{2}[x(n)\mathrm{e}^{j\omega_{\mathrm{c}}n} + x^*(n)\mathrm{e}^{-j\omega_{\mathrm{c}}n}], \quad (1)$$

where ω_{c} is the RF carrier radian frequency, $x(n)$ is the envelope of the RF input signal, and $x(n)$ can be expressed as

$$x(n) = A(n)\mathrm{e}^{j\varphi(n)} = x_{\mathrm{I}}(n) + jx_{\mathrm{Q}}(n), \quad (2)$$

where $A(n)$ and $\varphi(n)$ are the amplitude and phase of the envelop, $x_{\mathrm{I}}(n)$ and $x_{\mathrm{Q}}(n)$ are the corresponding real and imaginary components. The LNA and mixer are both strong nonlinear devices with memory effects [13], [14], and are the main sources of RF nonlinearities. Therefore, we choose the well-known Hammerstein model (a memoryless nonlinear block followed by a linear filter) [23], to model the RF nonlinearities with the memory effect, as shown

$$\begin{aligned} y_{\mathrm{RF}}(n) &= h(n) * \sum_{k=1}^{K_1} a_k x_{\mathrm{RF}}^k(n) \\ &= h(n) * \sum_{k=1}^{K_1}\sum_{l=0}^{k} \frac{a_k}{2^k}\binom{k}{l} x^{k-l}(n)[x^*(n)]^l \mathrm{e}^{j\omega_{\mathrm{c}}n(k-2l)} \end{aligned} \quad (3)$$

where a_k is the parameter of the nonlinear function, K_1 is the nonlinear order, and $h(n)$ is the impulse response of the linear filter that represents the memory effect. The operation symbol $*$ denotes the convolution operator, and $\binom{k}{l}$ denotes the binomial coefficient.

When dealing with the I/Q mixer, it's important to take into account the I/Q imbalance as well as nonlinearities. Due to the imperfect phase shift of the local oscillator signal of the I/Q mixer, there is a phase mismatch of φ_{m}. Additionally, the I/Q mixer also suffers from a relative amplitude mismatch g_{m} between the I and Q branches [10], [21]. Thus, The mixer outputs of the I and Q branches can be modeled as

$$\begin{aligned} y_{\mathrm{M,I}} &= y_{\mathrm{RF}}(n) \cdot \cos(\omega_{\mathrm{c}} n) \\ y_{\mathrm{M,Q}} &= y_{\mathrm{RF}}(n) \cdot [-g_m \sin(\omega_{\mathrm{c}} n + \varphi_m)]. \end{aligned} \tag{4}$$

After the I/Q mixer, the I and Q branches are filtered by bandpass filters to remove high-frequency components and allow only BB components to pass. Therefore, the frequency component that satisfies the conditions $k = 2l + 1$ in equation (3) can enter the BB stage. In other words, even-order nonlinearities and harmonics of the RF center frequency in (3) are filtered. In simpler terms, the order k can be gathered into the set $\mathbf{\Omega} = \{k | 1 \le k \le K_1, k = odd\}$. Thereby, the BB stage inputs of the I and Q branches can be modeled as

$$\begin{aligned} x_{\mathrm{BB,I}}(n) &= h(n) * \sum_{k \in \mathbf{\Omega}} \frac{a_k}{2^k} \binom{k}{\frac{k-1}{2}} \left[x(n) x^*(n)\right]^{\frac{k-1}{2}} x_{\mathrm{I}}(n) \\ &= h(n) * \sum_{p=1}^{P} e_p A^{2(p-1)}(n) x_{\mathrm{I}}(n) \\ x_{\mathrm{BB,Q}}(n) &= h(n) * \sum_{p=1}^{P} e_p A^{2(p-1)}(n) g_m \begin{pmatrix} x_{\mathrm{Q}}(n) \cos\varphi_m \\ -x_{\mathrm{I}}(n) \sin\varphi_m \end{pmatrix} \end{aligned} \tag{5}$$

where $p = \frac{k+1}{2}$, and $e_k = \frac{a_k}{2^k}\binom{k}{\frac{k-1}{2}}$ is the modified nonlinear parameter that includes the contribution of scalar scaling coefficients multiplying the signal component.

In the BB stage, input signals will be physically separated into the I and Q branches, and processed by the BB amplifiers and ADCs. The I and Q branches may have different nonlinearities and responses since they contain physically separate components [22]. Thus, the BB nonlinearities of the I and Q branches should be modeled separately. The BB nonlinearities are the cascade of nonlinearities of components in the I and Q branches, respectively. These can be represented by the Wiener model (a linear filter followed by a static nonlinear function), which has been widely used for modeling memory nonlinear systems [23], written as

$$\begin{aligned} y_{\mathrm{I}}(n) &= \sum_{i=1}^{M_1} b_i \left[c(n) * x_{\mathrm{BB,I}}(n)\right]^i \\ y_{\mathrm{Q}}(n) &= \sum_{i=1}^{M_2} d_i \left[s(n) * x_{\mathrm{BB,Q}}(n)\right]^i \end{aligned} \tag{6}$$

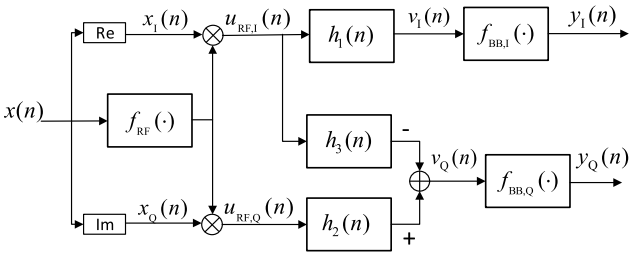

FIGURE 3. Block diagram of the proposed behavioral model of the DCR.

where b_i and d_i are the nonlinear parameters, M_1 and M_2 are the nonlinear orders of I and Q branches of the BB stage, and $c(n)$ and $s(n)$ are the impulse responses of I and Q branches respectively.

By combining the modeled RF nonlinearities, I/Q imbalance, and BB nonlinearities, we can obtain the model of the I and Q branches of the DCR, as shown in (7).

$$\begin{aligned} y_I(n) &= \sum_{i=1}^{M_1} b_i \left[c(n) * h(n) * \sum_{p=1}^{P} e_p A^{2(p-1)}(n) x_{\mathrm{I}}(n) \right]^i \\ &= \sum_{i=1}^{M_1} b_i \left[h_1(n) * \left(f_{\mathrm{RF}}[x(n)] x_{\mathrm{I}}(n)\right) \right]^i \\ y_Q(n) &= \sum_{i=1}^{M_2} d_i \Big[s(n) * h(n) * \sum_{p=1}^{P} e_p A^{2(p-1)}(n) g_m \\ &\qquad \times \left(x_{\mathrm{Q}}(n) \cos\varphi_m - x_{\mathrm{I}}(n) \sin\varphi_m\right) \Big]^i \\ &= \sum_{i=1}^{M_2} d_i \Big[h_2(n) * \left(f_{\mathrm{RF}}[x(n)] x_{\mathrm{Q}}(n)\right) - h_3(n) \\ &\qquad * \left(f_{\mathrm{RF}}[x(n)] x_{\mathrm{I}}(n)\right) \Big]^i \end{aligned} \tag{7}$$

where $f_{\mathrm{RF}}[x(n)] = \sum e_p A^{2(p-1)}(n)$, $h_1(n) = c(n) * h(n)$, $h_2(n) = s(n) * h(n) g_{\mathrm{m}} \cos\varphi_{\mathrm{m}}$, and $h_3(n) = s(n) * h(n) \sin\varphi_{\mathrm{m}}$.

The block diagram of the model is depicted in Fig. 3. We define $f_{\mathrm{RF}}[x(n)]$ as the RF nonlinear function. The BB nonlinear functions of I and Q branches are set as $f_{\mathrm{BB,I}}(\cdot) = \sum b_i(\cdot)^i$ and $f_{\mathrm{BB,Q}}(\cdot) = \sum d_i(\cdot)^i$, respectively. The parameters e_k, b_i, d_i of the functions $f_{\mathrm{RF}}(\cdot)$, $f_{\mathrm{BB,I}}(\cdot)$ and $f_{\mathrm{BB,Q}}(\cdot)$, as well as the impulse responses $h_1(n)$, $h_2(n)$, $h_3(n)$ are supposed to be estimated by the input-output data of the DCR.

III. MODEL PARAMETER ESTIMATION

Before applying the proposed model, it is important to estimate the model parameters by using the receiver's input-output data. This section presents a method for parameter estimation, which involves the inverse function approach, singular value decomposition (SVD), and least squares estimation. The procedure employs the receiver data set $\{x(n), y_{\mathrm{I}}(n), y_{\mathrm{Q}}(n)\}$ to determine the unknown parameters.

When using the inverse function, some clarification is necessary. First of all, the BB nonlinear functions of the I and Q branches $f_{\mathrm{BB,I}}(\cdot)$ and $f_{\mathrm{BB,Q}}(\cdot)$ are one-to-one and continuous, then the inverse functions $f^{-1}_{\mathrm{BB,I}}(\cdot)$ and $f^{-1}_{\mathrm{BB,Q}}(\cdot)$ exist and are also continuous. Moreover, its outputs $y_{\mathrm{I}}(n)$ and $y_{\mathrm{Q}}(n)$ are bounded and can be considered in a closed interval. According to the Stone-Wiestrass theorem, $f^{-1}_{\mathrm{BB,I}}(\cdot)$ and $f^{-1}_{\mathrm{BB,Q}}(\cdot)$ can be approximated to any desired precision by polynomials [24]. Thus, we construct these inverse functions as $f_{\mathrm{I}}^{-1}[y_{\mathrm{I}}(n)] = \sum r_i y^i_{\mathrm{BB,I}}(n)$ and $f^{-1}_{\mathrm{BB,Q}}[y_{\mathrm{Q}}(n)] = \sum s_i y^i_{\mathrm{Q}}(n)$.

Apply the inverse functions $f^{-1}_{\mathrm{BB,I}}(\cdot)$ and $f^{-1}_{\mathrm{BB,Q}}(\cdot)$ to (7), then

$$\begin{aligned}
\sum_{i=1}^{R_1} r_i y^i_{\mathrm{I}}(n) &= h_1(n) * \sum_{p=1}^{P} e_p A^{2(p-1)}(n) x_{\mathrm{I}}(n) \\
&= \sum_{q=0}^{Q_1} h_{1,q} \sum_{p=1}^{P} e_p x_{\mathrm{I},p}(n-q) \\
\sum_{i=1}^{R_2} s_i y^i_{\mathrm{Q}}(n) &= h_2(n) * \sum_{p=1}^{P} e_p x_{\mathrm{Q},p}(n) - h_3(n) * \sum_{p=1}^{P} e_p x_{\mathrm{I},p}(n) \\
&= \sum_{q=0}^{Q_2} h_{2,q} \sum_{p=1}^{P} e_p x_{\mathrm{Q},p}(n-q) \\
&\quad - \sum_{q=0}^{Q_3} h_{3,q} \sum_{p=1}^{P} e_p x_{\mathrm{I},p}(n-q)
\end{aligned} \tag{8}$$

where $h_{1,q}$, $h_{2,q}$ and $h_{3,q}$ are the parameters of the impulse response $\mathbf{h_1} = (h_{1,0}, \cdots, h_{1,Q_1})$, $\mathbf{h_2} = (h_{2,0}, \cdots, h_{2,Q_2})$and $\mathbf{h_3} = (h_{3,0}, \cdots, h_{3,Q_3})$.

Without loss of generality, set $r_1 = 1$ and $s_1 = 1$, then

$$\begin{aligned}
y_{\mathrm{I}}(n) &= -\sum_{i=2}^{R_1} r_i y^i_{\mathrm{I}}(n) + \sum_{q=0}^{Q_1} h_{1,q} \sum_{p=1}^{P} e_p x_{\mathrm{I},p}(n-q) \\
y_{\mathrm{Q}}(n) &= -\sum_{i=2}^{R_2} s_i y^i_{\mathrm{Q}}(n) + \sum_{q=0}^{Q_2} h_{2,q} \sum_{p=1}^{P} e_p x_{\mathrm{Q},p}(n-q) \\
&\quad - \sum_{q=0}^{Q_3} h_{3,q} \sum_{p=1}^{P} e_p x_{\mathrm{I},p}(n-q)
\end{aligned} \tag{9}$$

Define,

$$\begin{aligned}
\boldsymbol{\Phi}(n) &= \Big(-y^2_{\mathrm{I}}(n), \cdots, -y^{R_1}_{\mathrm{I}}(n), x_{\mathrm{I},1}(n), \cdots, x_{\mathrm{I},P}(n), \\
&\quad \cdots, x_{\mathrm{I},1}(n-Q_1) \cdots, x_{\mathrm{I},P}(n-Q_1)\Big)^{\mathrm{T}} \\
\boldsymbol{\theta} &= \big(r_2, \cdots, r_{R_1}, h_{1,0}e_1, \cdots, h_{1,0}e_P, \cdots, h_{1,Q_1}e_1, \\
&\quad \cdots, h_{1,Q_1}e_P\big)^{\mathrm{T}} \\
\boldsymbol{\Phi}_N &= (\boldsymbol{\Phi}(1), \boldsymbol{\Phi}(2), \cdots, \boldsymbol{\Phi}(N))^{\mathrm{T}} \\
\mathbf{Y}_{\mathrm{I},N} &= (y_{\mathrm{I}}(1), y_{\mathrm{I}}(2), \cdots, y_{\mathrm{I}}(N))^{\mathrm{T}}
\end{aligned} \tag{10}$$

then

$$\mathbf{Y}_{\mathrm{I},N} = \boldsymbol{\Phi}_N \boldsymbol{\theta}. \tag{11}$$

By using the receiver data set $\{x(n), y_{\mathrm{I}}(n)\}_{n=1}^{N}$, the parameter vector $\boldsymbol{\theta}$ can be estimated by the least square estimation [25]

$$\widehat{\boldsymbol{\theta}} = \left(\boldsymbol{\Phi}_N^{\mathrm{T}} \boldsymbol{\Phi}_N\right)^{-1} \boldsymbol{\Phi}_N^{\mathrm{T}} \mathbf{Y}_{\mathrm{I},N}. \tag{12}$$

Consequently, the estimated parameter vector $\widehat{\mathbf{r}} = (\widehat{r_1}, \cdots, \widehat{r_{R_1}})$ of the inverse function $f^{-1}_{\mathrm{BB,I}}(\cdot)$ can be obtained from $\widehat{\boldsymbol{\theta}}$.

Furthermore, for the estimated parameter $\widehat{h_{1p}e_k}$ in $\widehat{\boldsymbol{\theta}}$, we can use the SVD decomposition to solve the parameter vectors $\widehat{\mathbf{h_1}} = (\widehat{h_{1,0}}, \cdots, \widehat{h_{1,Q_1}})$ and $\widehat{\mathbf{e}} = (\widehat{e_1}, \cdots, \widehat{e_{Q_1}})$. We set

$$\boldsymbol{\Theta}_{h_1 e}(N) = \begin{bmatrix} \widehat{h_{1,0}e_1} & \cdots & \widehat{h_{1,0}e_P} \\ \vdots & \ddots & \vdots \\ \widehat{h_{1,Q_1}e_1} & \cdots & \widehat{h_{1,Q_1}e_P} \end{bmatrix}. \tag{13}$$

By making the SVD decomposition of $\boldsymbol{\Theta}_{h_1 e}(N)$, then

$$\boldsymbol{\Theta}_{h_1 \tilde{a}}(N) = \sum_{i=1}^{\min(m,n)} \boldsymbol{\mu_i} \sigma_i \boldsymbol{\nu}_i^{\mathrm{T}}. \tag{14}$$

We obtain the singular value σ_i, and the left and right singular vectors $\boldsymbol{\mu_i}$ and $\boldsymbol{\nu}_i$. The parameter vectors $\mathbf{h_1}$ and $\mathbf{e}$ can be estimated by

$$\widehat{\mathbf{h_1}} = s_\mu \boldsymbol{\mu_1}, \widehat{\mathbf{e}} = s_\mu \sigma_1 \boldsymbol{\nu_1}, \tag{15}$$

in which s_μ is the sign of the σ_1.

Define $u_{\mathrm{I}}(n) = \sum_{p=1}^{P} e_p x_{\mathrm{I},p}(n)$, $u_{\mathrm{Q}}(n) = \sum_{p=1}^{P} e_p x_{\mathrm{Q},p}(n)$, and

$$\begin{aligned}
\boldsymbol{\Psi}(n) &= \Big(-y^2_{\mathrm{Q}}(n), \cdots, -y^{R_2}_{\mathrm{Q}}(n), u_{\mathrm{Q}}(n), \cdots, u_{\mathrm{Q}}(n-Q_2) \\
&\quad -u_{\mathrm{I}}(n), \cdots, -u_{\mathrm{I}}(n-Q_3)\Big)^{\mathrm{T}} \\
\boldsymbol{\eta} &= \big(s_2, \cdots, s_{R_2}, h_{2,0}, \cdots, h_{2,Q_2}, \cdots, h_{3,0}, \cdots, h_{3,Q_3}\big)^{\mathrm{T}} \\
\mathbf{Y}_{\mathrm{Q},N} &= \big(y_{\mathrm{Q}}(1), \cdots, y_{\mathrm{Q}}(N)\big)^{\mathrm{T}}, \boldsymbol{\Psi}_N = (\boldsymbol{\Psi}(1) \cdots, \boldsymbol{\Psi}(N))^{\mathrm{T}}
\end{aligned} \tag{16}$$

then,

$$\mathbf{Y}_{\mathrm{Q},N} = \Psi_N \boldsymbol{\eta}. \tag{17}$$

With the receiver data set $\{x(n), y_{\mathrm{Q}}(n)\}_{n=1}^{N}$ and the estimated vector $\widehat{\mathbf{e}}$, the vectors $\mathbf{Y}_{\mathrm{Q},N}$ and $\boldsymbol{\Psi}_N$ can be calculated. Then the parameter vector $\boldsymbol{\eta}$ can be estimated by

$$\widehat{\boldsymbol{\eta}} = \left(\boldsymbol{\Psi}_N^{\mathrm{T}} \boldsymbol{\Psi}_N\right)^{-1} \boldsymbol{\Psi}_N^{\mathrm{T}} \mathbf{Y}_{\mathrm{Q},N}. \tag{18}$$

From $\widehat{\boldsymbol{\eta}}$, we can obtain the estimated parameters $\widehat{\mathbf{s}} = (\widehat{s_1}, \cdots, \widehat{s_{M_2}})$ of the inverse function $f^{-1}_{\mathrm{BB,Q}}(\cdot)$, and $\widehat{\mathbf{h_2}} = (\widehat{h_{2,0}}, \cdots, \widehat{h_{2,Q_2}})$ and $\widehat{\mathbf{h_3}} = (\widehat{h_{3,0}}, \cdots, \widehat{h_{3,Q_3}})$ of the impluse responses $h_2(n)$ and $h_3(n)$.

For the parameter vectors $\mathbf{b} = (b_1, b_2, \cdots, b_{M_1})$ and $\mathbf{d} = (d_1, d_2, \cdots, d_{M_1})$ of the functions $f_{\mathrm{BB,I}}(\cdot)$ and $f_{\mathrm{BB,Q}}(\cdot)$, it can

be obtained by using the estimated vectors $\widehat{\mathbf{r}}$ and $\widehat{\mathbf{s}}$, as shown in (18)

$$\widehat{\mathbf{b}} = \arg\min \sum_{n=1}^{N} \left\{ y_{\mathrm{I}}(n) - \sum_{m=1}^{M_1} b_m \Big(\sum_{i=1}^{R_1} \widehat{r}_i y_I^i(n) \Big)^m \right\}^2,$$
$$\widehat{\mathbf{d}} = \arg\min \sum_{n=1}^{N} \left\{ y_{\mathrm{Q}}(n) - \sum_{m=1}^{M_2} d_m \Big(\sum_{i=1}^{R_2} \widehat{s}_i y_Q^i(n) \Big)^m \right\}^2. \quad (19)$$

Above all, the proposed model parameters $\widehat{\mathbf{e}}$, $\widehat{\mathbf{b}}$, $\widehat{\mathbf{d}}$ of the functions $f_{\mathrm{RF}}(\cdot)$, $f_{\mathrm{BB,I}}(\cdot)$ and $f_{\mathrm{BB,Q}}(\cdot)$, and $\widehat{\mathbf{h_1}}$, $\widehat{\mathbf{h_2}}$ and $\widehat{\mathbf{h_3}}$ of the impluse responses $h_1(n)$, $h_2(n)$, $h_3(n)$ are estimated.

IV. EXPERIMENT RESULTS AND DISCUSSION

A. EXPERIMENT SETUP

To assess the effectiveness of the proposed model, we conducted experiments on a real RX chain. The RX chain is a typical DCR front-end that includes components such as LNA, I/Q mixer, filters, BB amplifiers, and ADCs, as shown in Fig. 4(a). The LNA is a high gain block amplifier of TQP3M9008 of Qorvo Cor. with a gain of 20.6 dB, the I/Q mixer is a broadband quadrature I-Q demodulator of the Analog Devices ADL5380, and the BB amplifier is the Analog Devices AD8130. The ADCs of the I and Q branches are both of AD9235. In addition to these commercial components, some bandpass and lowpass filters are also used in the RX chain. The experimental setup is established in Fig. 4(b), which includes two vector signal generators (Keysight N5166B and Agilent E8267D), an arbitrary waveform generator (RIGOL DG5351), a spectrum analyzer (R&S FSL18), and the FPGA board connected to the PC. In the experiment, we set the RX chain to work with the center frequency of 950 MHz. The flow diagram of the experiment and model simulation is shown in Fig.5.

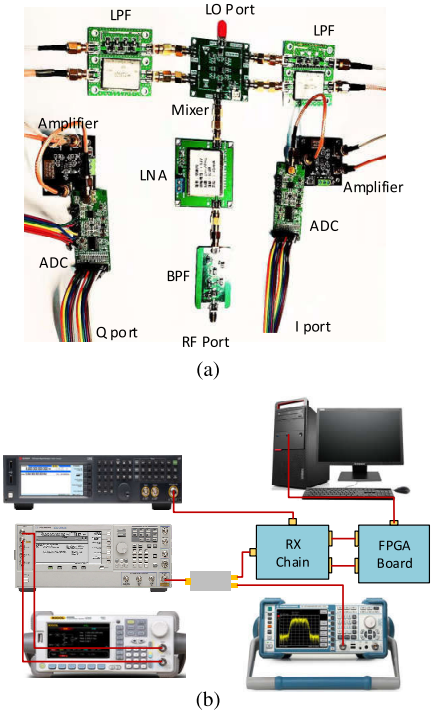

FIGURE 4. Experimental setup (a) picture of experimental RX chain (b) measurement setup.

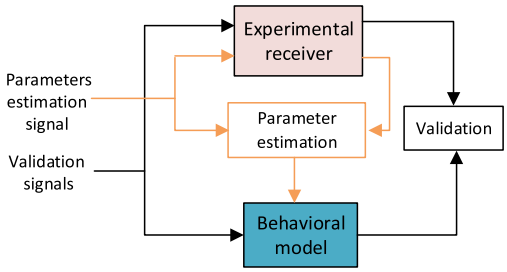

FIGURE 5. Flow diagram for experiment and model simulation.

B. RESULTS AND DISCUSSION

For better estimation of model parameters, the receiver data set should represent the nonlinear characteristics of the receiver as much as possible. Because input power levels are directly related to receiver nonlinearity, the higher power levels cause deeper nonlinearity in the receiver. For cases where the receiver is interfered with by strong block signals, intended or unintended, we need to construct a model that can accurately regenerate the nonlinear distortions caused by strong signals. Therefore, to enhance the range of nonlinearity degree of the model for nonlinear distortion regeneration, we use a WCDMA signal with a high power of -10 dBm and a peak-to-average power ratio of 9.65 dB as input for model parameter estimation. In this experiment, the I and Q branch outputs from the experimental RX chain were obtained as $y_I(n)$ and $y_Q(n)$, respectively. The model parameters of the RX chain were then estimated in MATLAB using the parameter estimation method outlined in section II.

As shown in Fig. 6(a), the power spectral densities (PSDs) of the input and output WCDMA signals of the RX chain are depicted by the blue dash-dotted curve and the black solid curve, respectively. The red-dotted curve represents the PSD of the proposed model with the estimated parameters. The output signal of the RX chain shows significant nonlinear distortions and spectrum regrowth compared to the input signal. Moreover, the output of the proposed model closely matches that of the RX chain. Fig. 6(b) displays the output waveforms of the I and Q branches of both the proposed model and RX chain. The waveforms of both branches have NMSEs below −48 dB, indicating that the model parameters have been accurately estimated.

After estimating the model parameters, we obtained the behavioral model for the RX chain. To evaluate the model's accuracy in reproducing the nonlinearity of the RX chain, we used various validation input signals that were different from the signal used for the model parameter estimation. It is important to note that the receiver nonlinearity is closely related to the input power levels. In order to validate the model's accuracy in reproducing different levels of nonlinearity of the RX chain, we used −5 dBm and −15 dBm

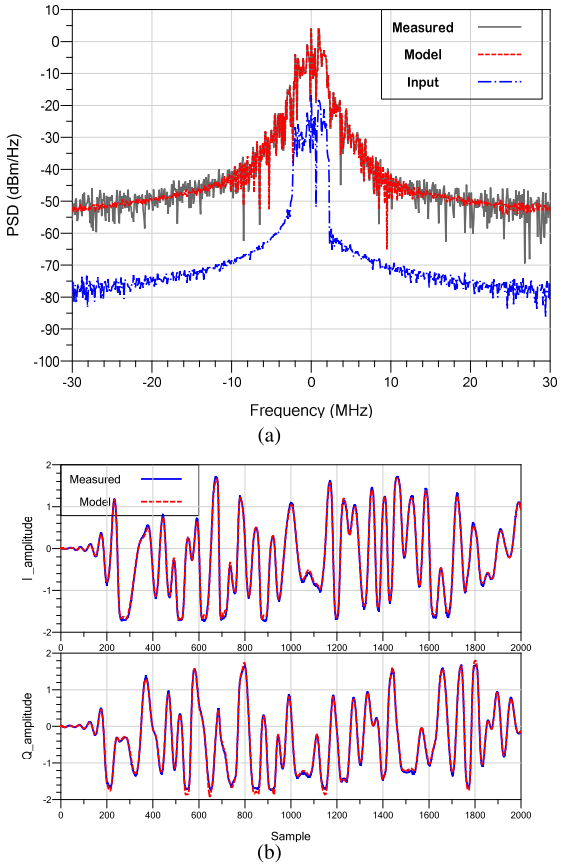

FIGURE 6. Parameter estimation results (a) PSDs (b) waveforms of the I and Q branches.

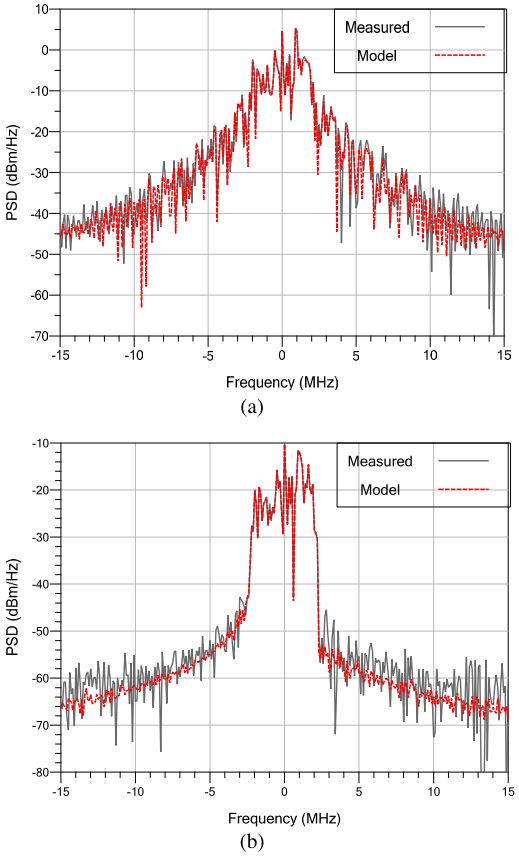

FIGURE 7. PSDs with WCDMA inputs of different power levels (a)−5 dBm (b) −30 dBm.

WCDMA signals, respectively, which were stronger and weaker than the signal used for parameter estimation, as validation signals.

Fig. 7 shows the output PSDs of the experimental measurement and model simulation. When the input is −5 dBm, the PSD has obvious spectral regrowth. On the other hand, when the input is −30 dBm, the output nonlinearity is weak due to the small power level. Nevertheless, the model's simulation results are consistent with the experimental measurement, regardless of the input signal's power level. This suggests that the model has good accuracy in regenerating different levels of the RX chain nonlinearity.

On the other hand, for the validation of the model's accuracy in reproducing intermodulation products, a 3-carrier WCDMA test signal with 3GPP standard at −15 dBm was used as the validation signal. The PSD results obtained from both the experimental measurement and model simulation are shown in Fig. 8. It is evident that the output exhibits self-distortions of carriers, as well as intermodulation distortions (IMDs). The simulation result of the behavioral model is in agreement with the experimental measurements. Table 1 displays the output powers of the main carriers and IMDs. The signal bandwidth for the 3-carrier WCDMA is 15 MHz, and each IMD has a bandwidth of 5 MHz. The powers of

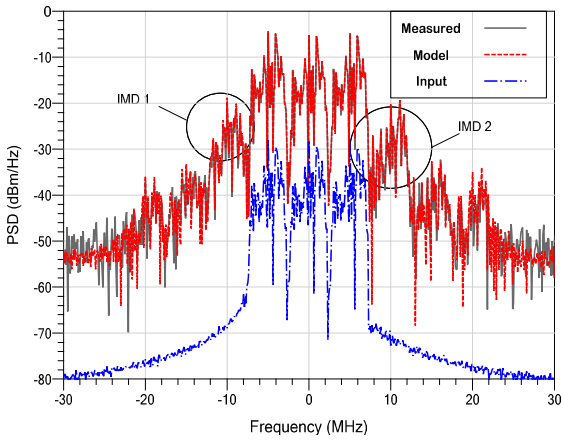

FIGURE 8. PSDs with the input of three-carrier WCDMA signal.

IMDs reproduced by the proposed model are very close to those measured in the experiment.

Moreover, in order to evaluate the universality of the proposed model, the OFDM modulated signal, another type of high PAPR modulation signal, has been applied for model validation. As shown in Fig. 9(a), the input OFDM signal is generated with a bandwidth of 10 MHz, the data rate is 6 MHz and the input power is set as −15 dBm. The PAPR of the

TABLE 1. Powers of main carriers and IMDs.

Terms	Main carriers	IMD 1	IMD 2
Measured (dBm)	8.14	−10.35	−10.77
Model (dBm)	8.23	−10.11	−10.71

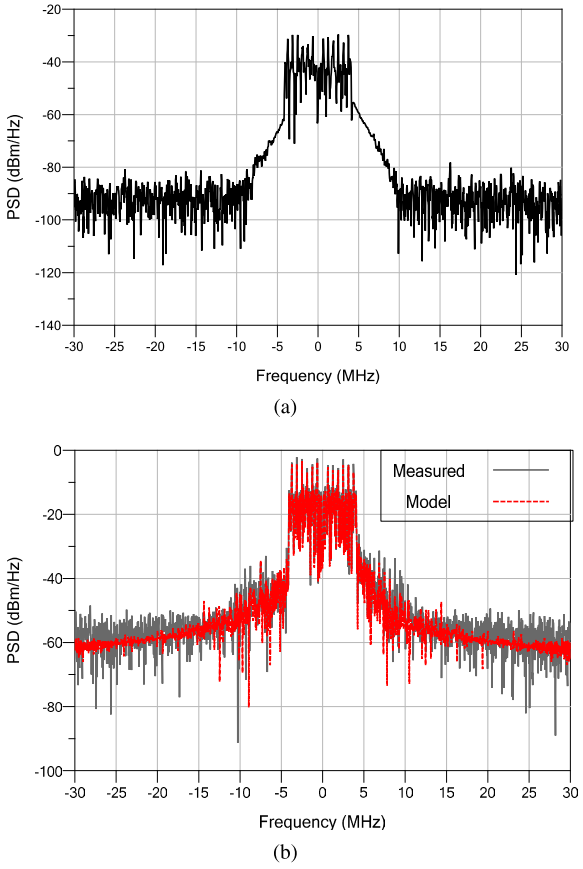

FIGURE 9. PSDs with the input of OFDM modulated signal.(a) OFDM modulated input signals (b) measured and simulated output PSDs.

input OFDM waveform is 6.83 dB. The output PSDs of the measurement and model simulation are shown in Fig. 9(b). The results show that the output has obvious distortions, and the adjacent bands are occupied by some nonlinear products. Meanwhile, the output of the model simulation is in good agreement with the measured. Therefore, for the different types of modulation signals, the proposed model can also make a good regeneration of output nonlinear distortions.

In practice scenarios, a DCR may simultaneously receive multiple signals with different modulations and powers. When these signals contain both strong and weak signals, the nonlinear products of strong signals may distort or mask the weak desired signal and occupy other channels. Therefore, it is essential to ensure that the model accurately reproduces the nonlinear distortion of this scenario. To simulate the multiple input signals, we have used three different modulated signals, as shown in Fig. 10(a).

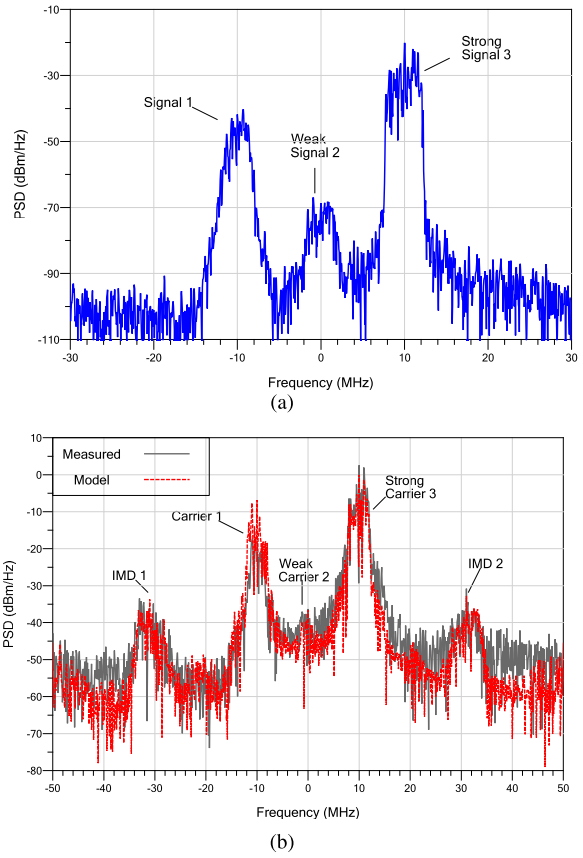

FIGURE 10. PSDs with the input of multiple modulated signals (a) multiple modulated input signals (b) measured and simulated output PSDs.

TABLE 2. Powers of distorted signals and IMDs.

Terms	Signal 1	Signal 2	Signal 3	IMD 1	IMD 2
Measured (dBm)	−6.1	−22.9	10.6	−22.6	−34.2
Model (dBm)	−5.8	−23.3	10.4	−23.1	−34.5

Signal 1 is a BPSK signal with a power of −25 dBm. Signal 2 is a weak QPSK signal with a power of −50 dBm. Signal 3 is a strong WCDMA signal with a power of −15 dBm. Fig. 10(b) shows the output power spectral densities (PSDs) of the experiment measurement and model simulation. The outputs exhibit noticeable nonlinear distortions, and the nonlinear products mask the weak signal 2. Furthermore, many other frequency bands also emerge with various nonlinear distortions, including the nonlinear products IMD 1 and IMD 2. It is evident that the nonlinear distortions in model reproduction are in good agreement with experimental measurements.

We also conducted a quantitative analysis of the nonlinear distortion to assess the accuracy of the model. Both of the channel powers of the distorted signals and IMDs are calculated and listed in Table 2. The channel bandwidth for each signal and IMD is set as 5 MHz during the calculation. The table data shows very small errors between the model reproductions and experimental measurements for both distorted signals and IMDs. Therefore, the model has

good reproduction of the nonlinear distortion of DCRs with the input containing several strong and weak signals, which is suitable for the nonlinear distortion mitigation.

V. CONCLUSION

This paper presents a nonlinear behavioral model of DCRs that can accurately reproduce the signal distortions and IMDs of the DCR with complex input signals and can be applied to the nonlinear distortions mitigation of receivers. This model characterizes the nonlinearities of the whole DCR front-end, which include arbitrary-order RF nonlinearities and BB nonlinearities, as well as the I/Q imbalance. Meanwhile, the method of model parameter estimation is proposed that involves the inverse function method, singular value decomposition (SVD) approach, and least square estimation. The experiment of an actual RX chain with the DCR structure is performed to validate this proposed model. In the experiment, a WCDMA signal is used to obtain the receiver data set for model parameter estimation. In addition, WCDMA signals with other power levels are used as the validation signals to evaluate the model in producing nonlinear distortions with inputs of different power levels. In the meantime, a three-carrier WCDMA signal is used to validate the model in reproducing IMDs of receivers. The measured and simulated results suggest that the model has an accurate reproduction of signal distortions and IMDs of the RX chain. For the purpose of validating the scenario where multiple signals, including a weak desired signal and strong signals, are received simultaneously, leading to interference from adjacent channels and masking of the weak signal, three signals with varying power levels and modulations are used as validation signals. The experimental and simulated results indicate that the proposed model has better accuracy in reproducing the signal distortions and IMDs for nonlinear distortion mitigation.

REFERENCES

[1] A. Dogra, R. K. Jha, and S. Jain, "A survey on beyond 5G network with the advent of 6G: Architecture and emerging technologies," *IEEE Access*, vol. 9, pp. 67512–67547, 2021.

[2] G. Hattab and M. Ibnkahla, "Multiband spectrum access: Great promises for future cognitive radio networks," *Proc. IEEE*, vol. 102, no. 3, pp. 282–306, Mar. 2014.

[3] C. Svensson, "The blocker challenge when implementing software defined radio receiver RF frontends," *Anal. Integr. Circuits Signal Process.*, vol. 64, no. 2, pp. 81–89, Aug. 2010.

[4] Z. Zhu, H. Leung, and X. Huang, "Challenges in reconfigurable radio transceivers and application of nonlinear signal processing for RF impairment mitigation," *IEEE Circuits Syst. Mag.*, vol. 13, no. 1, pp. 44–65, 1st Quart., 2013.

[5] Y. Chiu, "Equalization techniques for nonlinear analog circuits," *IEEE Commun. Mag.*, vol. 49, no. 4, pp. 132–139, Apr. 2011.

[6] E. A. Keehr and A. Hajimiri, "Digitally assisted equalization of third-order intermodulation products in wideband direct conversion receivers," *Int. J. Microw. Wireless Technol.*, vol. 1, no. 4, pp. 377–385, Aug. 2009.

[7] E. A. Keehr and A. Hajimiri, "Successive regeneration and adaptive cancellation of higher order intermodulation products in RF receivers," *IEEE Trans. Microw. Theory Techn.*, vol. 59, no. 5, pp. 1379–1396, May 2011.

[8] M. Valkama, A. S. H. Ghadam, L. Anttila, and M. Renfors, "Advanced digital signal processing techniques for compensation of nonlinear distortion in wideband multicarrier radio receivers," *IEEE Trans. Microw. Theory Techn.*, vol. 54, no. 6, pp. 2356–2366, Jun. 2006.

[9] J. Marttila, M. Allén, M. Kosunen, K. Stadius, J. Ryynänen, and M. Valkama, "Reference receiver enhanced digital linearization of wide-band direct-conversion receivers," *IEEE Trans. Microw. Theory Techn.*, vol. 65, no. 2, pp. 607–620, Feb. 2017.

[10] M. Grimm, M. Allén, J. Marttila, M. Valkama, and R. Thomä, "Joint mitigation of nonlinear RF and baseband distortions in wideband direct-conversion receivers," *IEEE Trans. Microw. Theory Techn.*, vol. 62, no. 1, pp. 166–182, Jan. 2014.

[11] E. Rebeiz, A. Shahed Hagh Ghadam, M. Valkama, and D. Cabric, "Spectrum sensing under RF non-linearities: Performance analysis and DSP-enhanced receivers," *IEEE Trans. Signal Process.*, vol. 63, no. 8, pp. 1950–1964, Apr. 2015.

[12] F. M. Ghannouchi and O. Hammi, "Behavioral modeling and predistortion," *IEEE Microw. Mag.*, vol. 10, no. 7, pp. 52–64, Dec. 2009.

[13] A. Borel, V. Barzdenas, and A. Vasjanov, "Linearization as a solution for power amplifier imperfections: A review of methods," *Electronics*, vol. 10, no. 9, p. 1073, May 2021.

[14] J. C. Pedro and S. A. Maas, "A comparative overview of microwave and wireless power-amplifier behavioral modeling approaches," *IEEE Trans. Microw. Theory Techn.*, vol. 53, no. 4, pp. 1150–1163, Apr. 2005.

[15] C. Peréz-Wences, J. R. Loo-Yau, P. Moreno, and J. A. Reynoso-Hernández, "Digital predistortion of RF power amplifier using the NARX-SVR model," *IEEE Microw. Wireless Technol. Lett.*, vol. 33, no. 4, pp. 475–478, Apr. 2023.

[16] A. Pedross-Engel, H. Schumacher, and K. Witrisal, "Modeling and identification of ultra-wideband analog multipliers," *IEEE Trans. Circuits Syst. I, Reg. Papers*, vol. 65, no. 1, pp. 283–292, Jan. 2018.

[17] M. Allén, J. Marttila, and M. Valkama, "Modeling and mitigation of nonlinear distortion in wideband A/D converters for cognitive radio receivers," *Int. J. Microw. Wireless Technol.*, vol. 2, no. 2, pp. 183–192, Apr. 2010.

[18] E. A. Keehr and A. Hajimiri, "Equalization of third-order intermodulation products in wideband direct conversion receivers," *IEEE J. Solid-State Circuits*, vol. 43, no. 12, pp. 2853–2867, Dec. 2008.

[19] X. Zhang, Y. Xia, C. Li, L. Yang, and D. P. Mandic, "Complex properness inspired blind adaptive frequency-dependent I/Q imbalance compensation for wideband direct-conversion receivers," *IEEE Trans. Wireless Commun.*, vol. 19, no. 9, pp. 5982–5992, Sep. 2020.

[20] X. Peng, F. Yu, Z. Wang, J. Liu, C. Wang, and J. Wang, "A frequency-domain I/Q imbalance calibration algorithm for wideband direct conversion receivers using low-cost compensator," *IEEE Access*, vol. 11, pp. 48739–48748, 2023.

[21] C. Chen, H. Lu, Y. Zhang, and G. Zhang, "Behavioral modeling for nonlinear effects of receiver front-ends based on block-oriented structure," *Prog. Electromagn. Res. C*, vol. 115, pp. 205–217, 2021.

[22] K. Wang, H. Lu, C. Chen, and Y. Xiong, "Modeling of system-level conducted EMI of the high-voltage electric drive system in electric vehicles," *IEEE Trans. Electromagn. Compat.*, vol. 64, no. 3, pp. 741–749, Jun. 2022.

[23] E. Bai and G. Fouad, *Block Oriented Nonlinear System Identification*. London, U.K.: Springer, 2010.

[24] V. Mathews and J. Sicuranza, *Polynomial Signal Processing*. New York, NY, USA: Wiley, 2000.

[25] P. Drineas, M. W. Mahoney, S. Muthukrishnan, and T. Sarlós, "Faster least squares approximation," *Numerische Math.*, vol. 117, no. 2, pp. 219–249, Feb. 2011.

CHONGCHONG CHEN received the B.E. degree in electronic information engineering from the School of Electronic Engineering, Xidian University, Xi'an, China, in 2015, and the master's degree in electromagnetic and microwave technology from Xidian University, in 2018, where he is currently pursuing the Ph.D. degree in electromagnetic and microwave technology. From 2018 to 2021, he studied electromagnetic compatibility and electromagnetic fields, and microwave technology. His current research interests include the electromagnetic compatibility and nonlinear behavioral model of nonlinear RF devices and systems.

HONGMIN LU (Member, IEEE) received the bachelor's and M.Eng. degrees in electromagnetic and microwave technology from Xidian University (former Northwest Telecommunication Engineering Institute), Xi'an, China, in 1981 and 1993, respectively, and the Ph.D. degree in electronic science and technology from Xi'an Jiaotong University, Xi'an, in 2000. In 1981, he joined the School of Electronic Engineering, Xidian University. He is currently a Professor with the Department of Microwave Telecommunication, the Director of the Key Laboratory of Ultra-High-Speed Circuits and Electromagnetic Compatibility, and an Invited Professor with the National Key Laboratory of Electromagnetic Compatibility. He has been engaged in the research of theoretical and applied electromagnetism, exposure protection, and electromagnetic compatibility in high-speed circuits. He conducted research on suppressing simultaneous switching noise using bandgap structures and metallic enclosures to shield apparatus over the past few years. His current research interests include electromagnetic compatibility (EMC) of vehicles and electromagnetic environmental effects (E3) and protection.

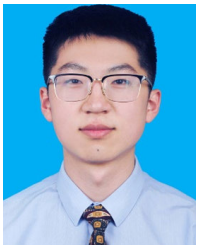

FULIN WU received the B.E. degree in electromagnetic and radio technology from the Xi'an University of Posts and Telecommunications, Xi'an, China, in 2019, and the M.S. degree in electronic science and technology from Xidian University, in 2021, where he is currently pursuing the Ph.D. degree in electromagnetic and microwave technology. His current research interests include wideband passive devices and antenna design, specifically the development of high-power components.

XUAN LIU received the B.E. degree in information security from the Xi'an University of Posts and Telecommunications, Xi'an, China, in 2010, and the M.S. degree in communication engineering from Xidian University, in 2013, where he is currently pursuing the Ph.D. degree in electromagnetic and microwave technology. He has long been engaged in satellite communication, satellite navigation technology research and payload product engineering development, and participated in a number of major national engineering tasks. His current research interests include high-sensitivity reception techniques for deep space communications and phased array adaptive acquisition and tracking techniques.

YANGZHEN QIN received the B.E. degree in electronic information engineering from the School of Electronic Engineering, Xidian University, Xi'an, China, in 2020, and the M.S. degree in electronic information engineering from Xidian University, in 2022, where he is currently pursuing the Ph.D. degree in electromagnetic and microwave technology. His research interests include the design of antenna for electromagnetic compatibility measurements and the electromagnetic compatibility design of electric vehicles.